Organic & Biomolecular Chemistry

PAPER

View Article Online
View Journal | View Issue

Cite this: *Org. Biomol. Chem.*, 2018, **16**, 4101

Design of RGD–ATWLPPR peptide conjugates for the dual targeting of $\alpha_V\beta_3$ integrin and neuropilin-1†

Fabien Thoreau,[a,b] Laetitia Vanwonterghem,[b] Maxime Henry,[b] Jean-Luc Coll *[b] and Didier Boturyn *[a]

Received 19th March 2018,
Accepted 11th May 2018

DOI: 10.1039/c8ob00669e

rsc.li/obc

Targeting the tumour microenvironment is a promising strategy to detect and/or treat cancer. The design of selective compounds that co-target several receptors frequently overexpressed in solid tumours may allow a reliable and selective detection of tumours. Here we report the modular synthesis of compounds encompassing ligands of $\alpha_V\beta_3$ integrin and neuropilin-1 that are overexpressed in the tumour microenvironment. These compounds were then evaluated through cellular experiments and imaging of tumours in mice. We observed that the peptide that displays both ligands is more specifically accumulating in the tumours than in controls. Simultaneous interaction with $\alpha_V\beta_3$ integrin and NRP1 induces NRP1 stabilization at the cell membrane surface which is not observed with the co-injection of the controls.

Introduction

The design of compounds that target the tumour microenvironment represents a major goal for cancer diagnosis and/or therapy. Among well identified tumour markers, several overexpressed receptors are widely used as targets for cancer applications, such as $\alpha_V\beta_3$ integrin,[1] epidermal growth factor receptor (EGFR),[2] vascular endothelial growth factor receptor (VEGFR-2),[3] neuropilin-1 (NRP1),[4] and folate receptor (FR-α).[5] Particular attention was dedicated to the ligand-targeted delivery of therapeutics or imaging agents. To date, many ligands have been discovered, mainly peptides,[6] antibodies[7] and aptamers.[8] The benefit of these biomolecules lies in their high selectivity and affinity which is at least in the nanomolar range. Among these compounds, there are inherent limitations in the use of antibodies and aptamers due to their size decreasing tumour penetration, expensive production and arduous chemical functionalization.[9] In such a context, many cell-targeting peptides composed of a few amino acids were designed. In particular, several peptide ligands comprising the ubiquitous triad sequence RGD (Arg-Gly-Asp) were developed for the targeting of $\alpha_V\beta_3$ integrin which is overexpressed on endothelial cells during angiogenesis and on other tumour cells.[1,10,11] The majority of RGD peptides are currently developed for imaging applications such as optical fluorescence,[12–16] positron emission tomography (PET),[17–20] single photon emission computed tomography (SPECT),[21,22] and magnetic resonance imaging (MRI).[23–25] Some RGD compounds have already been used in clinical trials.[17,19,20,26] As multimeric ligands are prone to bind their receptor with an increased affinity compared to their corresponding monomer,[27] the design of macromolecules containing several RGD moieties has been reported.[28–32] Over the last few years, our group has shown the potential of a tetrameric RGD-containing compound for tumour imaging especially for fluorescence guided surgery.[33,34] To improve the imaging of the tumour border, we decided to design a macromolecule that combines $\alpha_V\beta_3$ integrin and NRP1 ligands, both overexpressed in the tumour microenvironment during the progression of malignant tumours.[35] NRP1 is a non-tyrosine kinase co-receptor of VEGFR-2[36] which, in addition to its direct interaction with VEGFR-2, can also physically and functionally interacts with several integrins such as β1, β8 and β3.[37–40] Targeting these two receptors simultaneously thus became attractive.[41,42]

For this purpose, we conjugated the tetrameric RGD peptide with the ATWLPPR (A7R) peptide ligand that binds to NRP1 through a combination of chemoselective oxime ligation and copper(I)-catalysed alkyne–azide cycloaddition (CuAAC) (Fig. 1).[43] *In vitro* and *in vivo* evaluations of conjugates were then carried out and compared directly with their counterparts.

[a]*Univ. Grenoble Alpes, CNRS, Department of Molecular Chemistry, UMR 5250, F-38000 Grenoble, France. E-mail: didier.boturyn@univ-grenoble-alpes.fr*
[b]*Univ. Grenoble Alpes, INSERM U1209 - UMR CNRS 5309, Institute for Advanced Biosciences, F-38700 Grenoble, France*

†Electronic supplementary information (ESI) available. See DOI: 10.1039/c8ob00669e

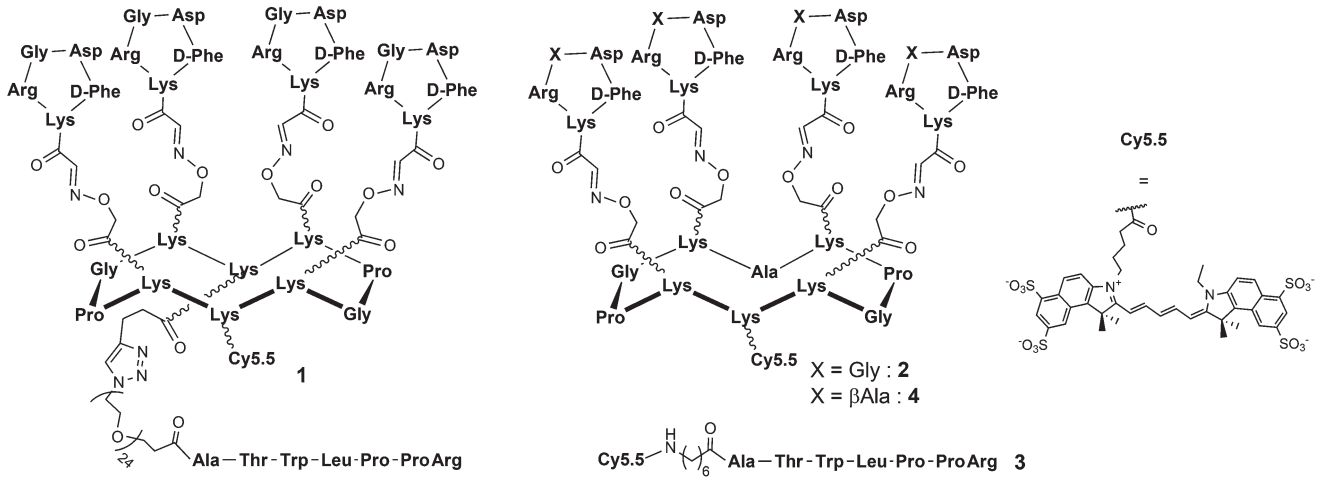

Fig. 1 Structures of compounds **1–4** comprising RGD and/or A7R peptide ligands.

Results and discussion

Design and synthesis of RGD–ATWLPPR peptide conjugates

For this study, we prepared compound **1** that displays the tetrameric RGD group and the A7R peptide ligand, the control peptides **2** and **3** that target respectively $\alpha_V\beta_3$ integrin and NRP1, and peptide **4** in order to confirm that the binding of the tetrameric RGD peptide is due to its selective integrin recognition and not through the interaction of the arginine residue (Fig. 1). To produce the macromolecule **1**, we used a convergent chemical synthesis through sequential chemoselective ligations of the functional units using oxime ligation and copper(I)-catalysed azide–alkyne cycloaddition (Scheme 1). By using a standard solid and solution-phase peptide synthesis, we first prepared the peptide intermediates **5**, **6** and **7** containing the prerequisite chemoselective functional groups such as, on the one hand, protected aminooxy and aldehyde functional groups, and, on the other hand, alkyne and azide functional groups. To include chemoselective functional groups within the cyclopeptides **5** and **6** during the solid-phase peptide synthesis (SPPS), we used building blocks consisting of lysine bearing on its side-chain alkyne a protected aminooxy functional group or a serine as a masked aldehyde functional group.[44] This considerably reduces the number of steps involved and the combination of protecting groups required for the synthesis of the functionalized peptides. With the trifunctional compound **5** in hand, we then carried out the sequential chemoselective ligations of different biomolecules (Scheme 1). Oxime ligation of RGD peptides **6** was carried out under mild acidic conditions that allow the deprotection of aminooxy and amine functional groups. Reversed-phase HPLC furnished the expected biomolecular compound in a yield of about 40%. The RGD-containing compound was then converted to the fluorescent intermediate simply by the addition of the NHS (*N*-hydroxysuccinimide) ester of a Cy5.5 fluorescent probe and obtained in a yield of 80% after purification. The subsequent chemoselective ligation was carried out under standard CuAAC conditions by using $CuSO_4$, ascorbate and THPTA (tris(3-hydroxypropyltriazolylmethyl)amine) ligand.[45] The fluorescent compound **1** was readily purified by reversed-phase HPLC in a yield of about 25% and characterized by mass spectrometry (see the ESI†).

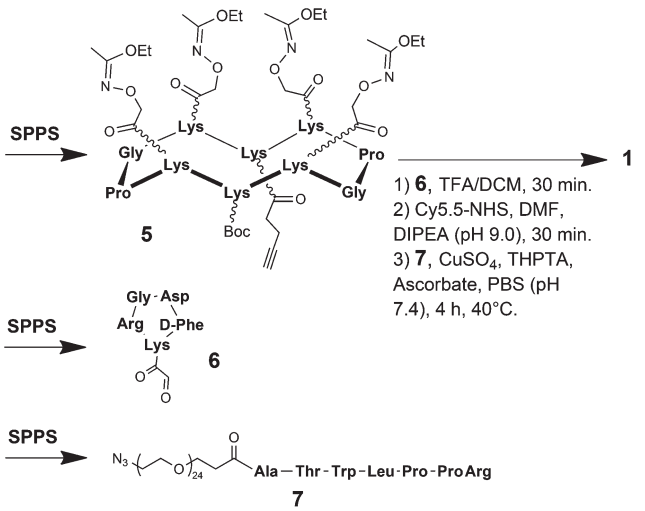

Scheme 1 Convergent chemical synthesis of multifunctional compound **1**.

In parallel, we prepared the control RGD-containing peptide **2** and the nonsense RβAD peptide **4** as previously described.[14] The control A7R-containing peptide **3** was directly obtained from SPPS. All compounds were purified by reversed-phase HPLC and identified by mass spectrometry (see the ESI†).

In vitro cellular experiments

In order to evaluate the binding and internalization of the different compounds *in vitro*, we incubated the different molecules at 2.5 μM with adherent human glioblastoma U87MG cells that express $\alpha_V\beta_3$ integrin and NRP1. As expected, the cells were strongly labelled with RGD peptide **2** (Fig. 2c) in

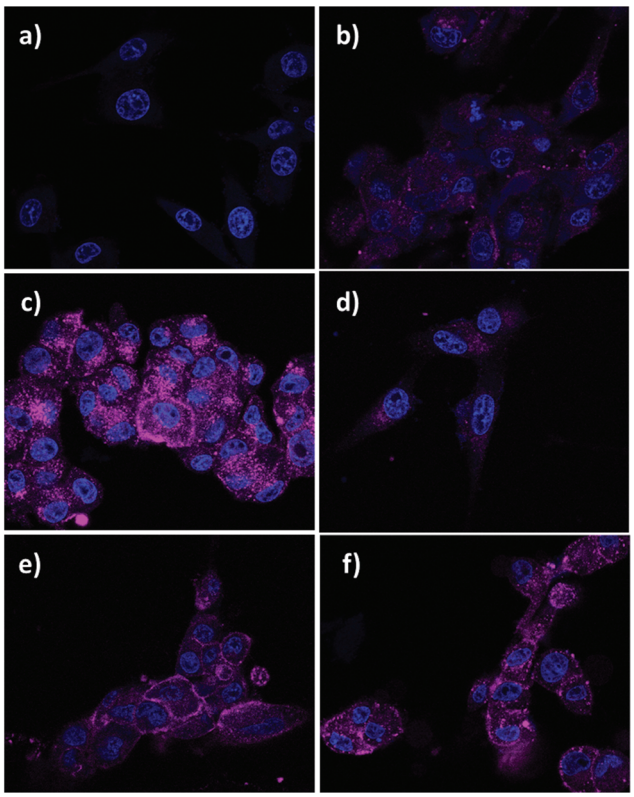

Fig. 2 Confocal microscopy images of U87MG cells. Cells were incubated for 30 min in (a–f) cell culture medium with (b) 2.5 μM compound **4**, (c) 2.5 μM compound **2**, (d) 2.5 μM compound **3**, (e) 2.5 μM compound **1**, and (f) 2.5 μM compound **2** and 2.5 μM compound **3**. Nuclei were stained in blue.

comparison with the RβAD compound **4** (Fig. 2b). In contrast, the A7R peptide **3** (Fig. 2d) or RGD–A7R peptide conjugate **1** (Fig. 2e) provided a less intense staining of the cells. As can be seen also in Fig. 2c and e, both compounds **2** and **1** were present on the cell surface, while RGD–A7R peptide conjugate **1** was sparsely present in the cytoplasm in comparison with compound **2** or a co-injection of peptides **2** and **3**. This suggests that the dual targeting of integrin and NRP1 reduces the internalization of RGD–A7R peptide conjugate **1**. Additionally, co-presentation of the two peptides does not augment the overall intensity of staining of the cells.

We then studied the variation in NRP1 contents after incubation of the cells with the different molecules (Fig. 3). As can be seen compared to untreated cells, all peptides except peptide conjugate **1** induced a significant degradation of NRP1. This diminution is due to NPR1 degradation after internalization in the presence of the peptides, except for RGD–A7R peptide conjugate **1**. In this case, the NRP1 receptor is protected from degradation, suggesting that the simultaneous recognition of NRP1 and integrin stabilizes NRP1 on the cell membrane. Not observed for the co-injection of compounds **2** and **3**, this phenomenon seems to be spatial-dependent confirming the interest to combine different ligands within the same compound.

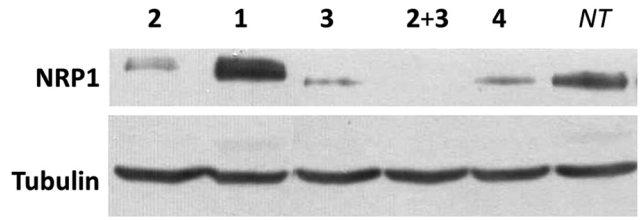

Fig. 3 The total amount of NRP1 and tubulin proteins was evaluated by western blotting. U87MG cells were incubated for 30 min in the presence of 1 μM of each compound (except the not-treated (NT) cells). The level of tubulin serves as an internal loading control.

The stabilization of NRP1 on the cell surface was then confirmed using the in-cell Elisa test (Fig. 4). In this case, the cells are treated with the peptides, and the presence of NRP1 on the extracellular part of the plasma membrane is detected by an antibody. As can be seen in Fig. 4, while the incubation with the RGD peptide **2** was associated with a reduction of 18% of the NRP1 level compared to control cells, the RGD–A7R peptide conjugate **1** stabilized NRP1 up to 122% of its natural level on the surface of the cells. The dual peptide thus prevents NRP1 natural turnover and/or active internalization.

Tumour imaging

After intravenous administration in mice bearing subcutaneous tumours, we observed that the compounds **1** and **2** stained very specifically the tumours (Fig. 5a and b) compared to the negative control compound **4** (Fig. 5c). Compound **1** seems to bind more strongly to the kidneys than compound **2** due to its augmented size. As expected and also based on our previous work, compounds that display 4 RGD or RβAD peptides were strongly captured by the kidneys during their evacuation in urine.

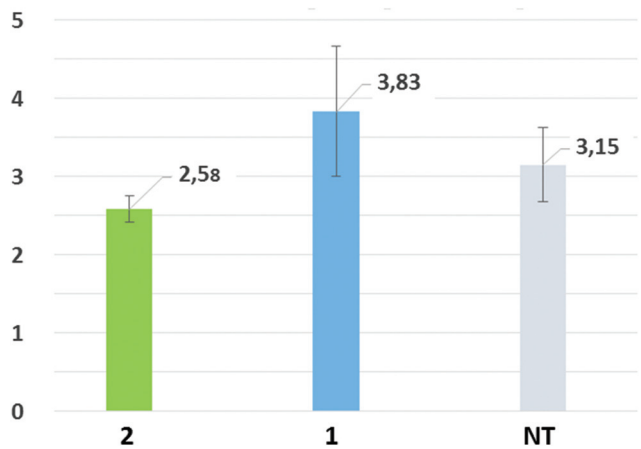

Fig. 4 The dual peptide stabilized the NRP1 protein on the surface of the cells as established by using an In-cell ELISA Assay. The cells were incubated for 30 min with compound **2** or compound **1** or without the peptide (NT). The presence of NRP1 on the cell surface was then tested using immunostaining with an anti-NRP1 antibody.

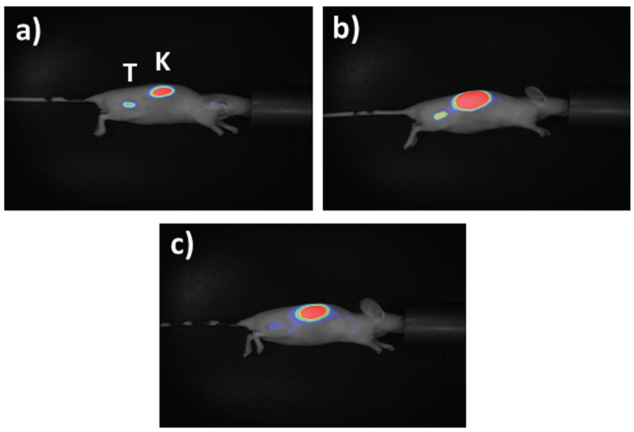

Fig. 5 Representative fluorescence images of Swiss nude mice bearing U87MG s.c. tumours after i.v. injection of 10 nmol Cy5.5-labeled (a) compound **2**, (b) compound **1**, and (c) compound **4**. Images were obtained 1.5 h after injection. T and K indicate tumour and kidneys, respectively.

As the signal was saturated in the kidneys, we did not calculate the tumour/kidney ratio. However, we were able to calculate the tumour/skin (T/S) ratio, which is a key parameter for imaging applications. It was obtained by drawing a region of interest (ROI) on the subcutaneous tumour and a similar ROI positioned on the skin of the back of the mouse. This T/S ratio, which reflects the contrast between the tumour and the surrounding normal skin, indicates that the RGD–A7R peptide conjugate **1** was more specifically accumulating in the tumours than RGD peptide **2** as early as 1.5 h after injection (Fig. 6). The T/S ratios which reflect the contrast seen on the images indicate that the RGD–A7R peptide conjugate **1** was more specifically accumulating in the tumours than RGD peptide **2** alone as early as 1.5 h after injection (Fig. 6). Note that the tumour/skin fluorescence ratio for **1** remains high until 24 h.

RGD peptides have been intensively investigated as targeting vectors in particular for tumour optical imaging.[46] We successfully exploited a tetrameric RGD compound for the near-infrared optical guided surgery of highly infiltrative fibrosarcomas in cats.[34] To improve the tumour targeting, some research groups have designed dual targeted conjugates based on the RGD peptide with VEGFR-1,[41] aminopeptidase N (CD13),[47] and NRP-1.[48,49] Our results show a faster and more specific accumulation of the dual targeted compound **1** than that of RGD control **2**. Altogether, *in vitro* and *in vivo* results suggest that the dual targeting of $\alpha_v\beta_3$ integrin and NRP1 receptors is associated with an increased binding, better selectivity and stabilized retention of the probe on the target cells and tumours.

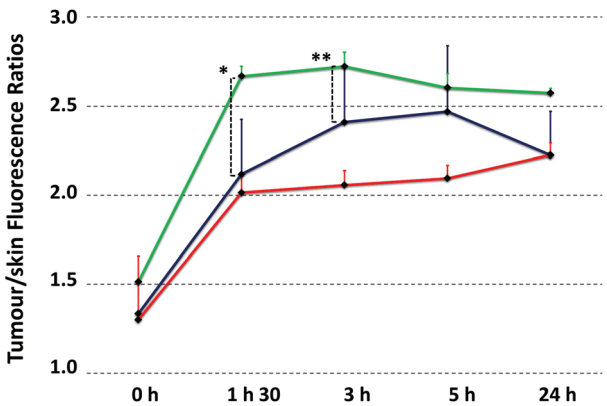

Fig. 6 Tumour/skin fluorescence ratios measured over a period of 24 h after the injection of fluorescent compound **1** (green curve), compound **2** (blue curve) and compound **4** (red curve). Asterisks indicate statistical significance; according to a two sample Student *t*-test: * $p < 0.05$, ** $p < 0.1$.

Conclusions

Single targeting of receptors overexpressed in tumours may eventually suffer from a reduced spatio-temporal presence or accessibility of the target receptor. Aiming at multiple targets is thus expected to lower this risk and augment the panel of tumours that may be detected. In the present work, we show that the design of a dual RGD–ATWLPPR peptide is indeed able to bind with an improved tumour/background ratio to tumour cells *in vitro* and *in vivo*. The development of such probes is expected to broaden the spectrum of tumours that will be detected, and thus to generate the second generation of molecular probes. Furthermore, we show that the combination of RGD and ATWLPPR ligands on a single molecule had a different biological impact on the corresponding receptors compared to their co-injection. These results encourage the design of new multi-targeting systems, as they could have unexpected biological implications in addition to their aforementioned advantages. The exploration of the combination of various cancer-aimed ligands could be of great interest for cancer imaging and/or therapy.

Experimental

Synthesis of peptide 5

Peptide **5** was obtained from the cyclization of a linear peptide (554 mg, 0.3 mmol) in DMF (0.5 mM) by using PyBOP (benzotriazol-1-yl-oxytripyrrolidinophosphonium hexafluorophosphate) reagent (1.2 equiv.) and DIPEA (diisopropylethylamine) to adjust the pH to 8.0. The reaction mixture was then stirred for 1 h. Precipitation from ether afforded cyclic peptide **5** as a light brown powder (550 mg, 0.3 μmol). This crude material was used without further purification.

Synthesis of aldehyde-containing RGD peptide 6

Cyclopentapeptide c[-Arg-Gly-Asp-DPhe-Lys(CO-CHO)-] **6** was obtained as previously described.[33]

Synthesis of azide-containing A7R peptide 7

The peptide was assembled on 2-chlorotrityl chloride resin (20 mg, loading of 0.54 mmol g^{-1}) using the standard Fmoc/*t*-Bu procedure and N_3-PEG_{24}-OH. The anchoring of the first

amino acid (Fmoc-Arg(Pbf)-OH) was performed following the standard procedure yielding a resin loading of 0.35 mmol g^{-1}. The protected peptide was released from the resin by using a solution containing TFA/CH_2Cl_2 (1/99), and stirred for 4 h by using a solution containing TFA/TIS/H_2O (95/2.5/2.5). The linear peptide **7** was obtained in 20% yield as a white powder after RP-HPLC and lyophilization (3.3 mg, 1.4 μmol).

Synthesis of peptide conjugate 1

Cyclodecapeptide **5** (20 mg, 11 μmol) and 6 equiv. of **6** (44 mg, 66 μmol) were dissolved in 1.2 mL of a TFA/H_2O (7/3) solution. The mixture was stirred for 30 min and the product was purified by RP-HPLC affording a pure RGD intermediate as a white powder in 41% yield (18 mg, 4.48 μmol).

The RGD intermediate (4.1 mg, 1 μmol) and 2 equiv. of tetrasulfo-Cy5.5-mono-NHS-ester (3.4 mg, 2 μmol) were dissolved in 2 mL of a DMF/DIPEA (pH = 9) solution. The mixture was stirred for 30 min and the product was purified by RP-HPLC affording a pure fluorescent RGD conjugate as a blue powder in 80% yield (3.2 mg, 0.8 μmol).

To a stirred solution of the fluorescent RGD conjugate (1.2 mg, 245 nmol) and peptide **7** (1.2 eq., 640 μg, 318 nmol) in 200 μL DMF/PBS (pH 7.4, 1 mM) (5/5) was added a solution of $CuSO_4$ (66 μg, 265 nmol, 1 eq.) and THPTA (345 μg, 795 nmol, 3 eq.) in 30 μL of PBS (pH 7.4, 1 mM). All solutions were degased under argon. To this blue stirred solution was added a solution of ascorbate (233 μg, 1.325 μmol, 5 eq.) in 30 μL PBS (pH 7.4, 1 mM). Both solutions were degased under argon. The uncoloured resulting solution is stirred for 4 h at 40 °C. The final compound **1** was obtained pure as a blue powder in 25% yield after RP-HPLC purification and lyophilization (420 μg, 61 nmol).

Synthesis of peptides 2 and 4

Peptides **2** and **4** were prepared as previously described with some modifications (see the ESI†).[14]

Synthesis of a fluorescent A7R peptide

A linear peptide was assembled on 2-chlorotrityl chloride resin (2 g, loading of 0.7 mmol g^{-1}). The anchoring of the first amino acid (Fmoc-Arg(Pbf)-OH) was performed manually following the standard procedure yielding a resin loading of 0.37 mmol g^{-1}. The peptide was released from the resin using a TFA/CH_2Cl_2 (99/1) cleavage solution and stirred for 4 h in a TFA/TIS/H_2O (95/2.5/2.5) deprotection solution. The linear peptide was obtained in 85% yield after RP-HPLC and lyophilization (600 mg, 630 μmol).

To a stirred mixture of the linear peptide (1.32 mg, 1.38 μmol) in DMF and DIPEA (pH = 9) was added 2 equiv. of tetrasulfo-Cy5.5-mono-NHS-ester (2.8 mg, 2.76 μmol). The dark blue solution was stirred for 1 h at room temperature. After the evaporation of solvents under reduced pressure, the crude product was purified by RP-HPLC, affording the product **3** as a dark blue powder in 70% yield after lyophilization (1.78 mg, 966 nmol).

Confocal microscopy

U87MG cells were seeded in an 8 well Lab Tek plate (20 000 cells in 40 μL of PBS Ca^{2+}/Mg^{2+} per well). 260 μL of DMEM 10% SVF were added and the cells were incubated overnight at 37 °C in 5% CO_2. After the removal of the medium and washing with PBS Mg^{2+}/Ca^{2+}, 0.50 nmol of compounds in 200 μL of PBS Mg^{2+}/Ca^{2+} (final concentration = 2.5 μM) were added on adherent cells. They were incubated for 30 min at 37 °C in 5% CO_2. Nuclei were labelled with a Hoechst colorant and the cells were fixed with 2% PFA. The cells were analysed by confocal microscopy with a Dynascope® (multiparametric confocal microscopy). Objectives: Plan apochromat 63 × 1.40 oil DICIII. Filters: O1 LP (for DAPI) and Cy5 (for Cy5.5). Images were analysed with Image J® (NIH software).

Western blotting

1 million U87MG adherent cells were incubated with 1 μM of a fluorescent compound (**1**, **2**, **3** or **4**), or a combination of compounds (**2** + **3**) each being at 1 μM, or PBS only, for 30 min at 37 °C. The cells were harvested, washed in PBS, and incubated in lysis buffer (10 mmol L^{-1} Tris–HCl (pH 7.5), 120 mmol L^{-1} NaCl, 1 mmol L^{-1} EDTA, 1 mmol L^{-1} dithiothreitol, 0.5% Nonidet P-40 and 0.05% sodium dodecyl sulfate, supplemented with protease and phosphatase inhibitors). After centrifugation at 13 000 rpm for 30 min at 4 °C, the protein containing supernatant is taken off. Protein content was assessed by using a Bio-Rad D C Protein Assay kit (Bio-Rad Laboratories, Ivry sur Seine, France). 20 μg of protein were loaded onto SDS polyacrylamide gel (12%). Migration is realised at 0.25 A and 200 V for 50 min. Transfer on nitrocellulose membranes is realised in 1 h 20 min at 0.20 A and 90 V. Western blotting was performed using anti-neuropilin-1 rabbit monoclonal antibody (Abcam #81321) and anti-tubulin mouse monoclonal antibody. To ensure equal loading and transfer, membranes were also probed for tubulin using anti-tubulin mouse monoclonal antibody (1/1000; Santa Cruz, #23948). Horseradish peroxidase conjugated anti-IgG antibodies were used as secondary antibodies. ECL solution (peroxidase substrate) was added and time-course exposure of proteins to chemiluminescence was used to perform the semi-quantification of the signal. The intensity of each band was measured using Image J® (NIH software).

In-cell ELISA test

The in-cell ELISA tests were performed using ThermoFisher In-cell ELISA kits® following the given ThermoFisher® procedure. U87MG cells were plated in a 96 well plate (10 000 cells per plate). After incubation with 1 μM of compounds **1**, **2** or PBS only, they were washed with PBS and fixed using a 4% PFA solution. Endogenous peroxidase was quenched and non-specific sites were blocked using the quenching solution and the blocking buffer from the kit. Half of the cells were incubated with anti-NRP1 antibody (1/1000, Abcam 81321) overnight at 4 °C. After washing, all the cells were incubated for 30 min with horseradish peroxidase conjugated secondary

antibody (anti-rabbit) at room temperature. After washing, the TMB substrate was added at room temperature and protected from light. The reaction was stopped after 15 min and the absorbance was measured at 450 nm.

The absorbance results had to be normalised. For this, the cells were washed and incubated with Janus Green Whole-Cell stain for 5 min at room temperature. After washing and 10 min of incubation with elution buffer from the kit, the absorbance was measured at 615 nm.

The absorbance measured at 450 nm in each well is divided by the values measured at 615 nm in the corresponding wells. The extracellular NRP1 expression levels are evaluated comparing the standardised absorbance values.

Tumour implantation and treatment

10 million U87MG cells, suspended in 200 μL PBS, were injected subcutaneously into female NMRI nude mice (6 weeks old). After 5 weeks, the animals were divided into four groups: group I (n = 6, S1 to S6) was administered compound **2**, group II (n = 6, S7 to S12) was administered compound **1**, group III (n = 3, S13 to S15) was administered compound **4**, and group IV (n = 2, S16 to S17) was administered compound **3**. 10 nmol of compound in 200 μL of PBS were injected into each mouse. Fluorescence imaging was realised with Hamamatsu® apparatus at t = 0 h, t = 1 h 30 min, t = 5 h or t = 24 h post injection. Mice S4 to S6 and S10 to S12 were sacrificed and dissected at t = 5 h, and the other mice were sacrificed and dissected at t = 24 h post injection. Organs and subcutaneous tumours were excised and imaged with a Hamamatsu® camera (see the ESI,† Fig. S25–S41). The fluorescence values obtained for the skin and tumour of each mouse were used to elaborate Fig. 6. For each mouse, the corrected fluorescence of the tumour was divided by the corrected fluorescence of the skin to give the "Tumour/Skin fluorescence ratio". To determine error bars, we first calculated for each group (*i.e.* mice treated with the same compound and sacrificed at the same time) the average tumour/skin fluorescence ratio of the group. Error bars correspond to the average of the absolute deviations of all individual tumour/skin fluorescence ratios from the average tumour/skin fluorescence ratio of the group.

Conflicts of interest

There are no conflicts to declare.

Acknowledgements

The authors wish to acknowledge the support from the ICMG Chemistry Nanobio Platform, Grenoble, on which peptide synthesis has been performed. This work was supported by the Agence Nationale de la Recherche LabEx "Arcane" (ANR-11-LABX-0003-01) and "Mimobody" (ANR-13-BS07-0014-01).

Notes and references

1 K. Temming, R. M. Schiffelers, G. Molema and R. J. Kok, *Drug Resist. Updates*, 2005, **8**, 381.
2 J. R. Woodburn, *Pharmacol. Ther.*, 1999, **82**, 241.
3 N. Ferrara, K. J. Hillan and W. Novotny, *Biochem. Biophys. Res. Commun.*, 2005, **333**, 328.
4 A. Starzec, R. Vassy, A. Martin, M. Lecouvey, M. Di Benedetto, M. Crépin and G. Y. Perret, *Life Sci.*, 2006, **79**, 2370.
5 P. Low, W. A. Shenne and D. D. Doorneweerd, *Acc. Chem. Res.*, 2007, **41**, 120.
6 E. Vivès, J. Schmidt and A. Pèlegrin, *Biochim. Biophys. Acta*, 2008, **1786**, 126.
7 A. M. Wu and P. D. Senter, *Nat. Biotechnol.*, 2005, **23**, 1137.
8 L. Cerchia and V. de Franciscis, *Trends Biotechnol.*, 2010, **28**, 517.
9 M. A. Firer and G. Gellerman, *J. Hematol. Oncol.*, 2012, **5**, 70.
10 E. Garanger, D. Boturyn and P. Dumy, *Anti-Cancer Agents Med. Chem.*, 2007, **7**, 552.
11 F. Danhier, A. Le Breton and V. Préat, *Mol. Pharmaceutics*, 2012, **9**, 2961.
12 Z. Cheng, Y. Wu, Z. Xiong, S. S. Gambhir and X. Chen, *Bioconjugate Chem.*, 2005, **16**, 1433.
13 Y. Ye, S. Bloch, B. Xu and S. J. Achilefu, *J. Med. Chem.*, 2006, **49**, 2268.
14 Z. Jin, V. Josserand, J. Razkin, E. Garanger, D. Boturyn, M.-C. Favrot, P. Dumy and J.-L. Coll, *Mol. Imaging*, 2006, **5**, 188.
15 Z. Jin, J. Razkin, V. Josserand, D. Boturyn, A. Grichine, I. Texier, M.-C. Favrot, P. Dumy and J.-L. Coll, *Mol. Imaging*, 2007, **6**, 43.
16 Z. Liu, S. Liu, G. Niu, F. Wang, S. Liu and X. Chen, *Mol. Imaging*, 2010, **9**, 21.
17 H. Chen, G. Niu, H. Wu and X. Chen, *Theranostics*, 2016, **6**, 78.
18 H. Cai and P. S. Conti, *J. Labelled Compd. Radiopharm.*, 2013, **56**, 264.
19 W. Wan, N. Guo, D. Pan, C. Yu, Y. Weng, S. Luo, H. Ding, Y. Xu, L. Wang, L. Lang, Q. Xie, M. Yang and X. Chen, *J. Nucl. Med.*, 2013, **54**, 691.
20 R. Haubner, W. A. Weber, A. J. Beer, E. Vabuliene, D. Reim, M. Sarbia, K.-F. Becker, M. Goebel, R. Hein, H.-J. Wester, H. Kessler and M. Schwaiger, *PLoS Med.*, 2005, **2**, e70.
21 Y. Zhou, S. Chakraborty and S. Liu, *Theranostics*, 2011, **1**, 58.
22 S. Liu, W.-Y. Hsieh, Y. Jiang, Y.-S. Kim, S. G. Sreerama, X. Chen, B. Jia and F. Wang, *Bioconjugate Chem.*, 2007, **18**, 438.
23 Y. Cui, C. Zhang, R. Luo, H. Liu, Z. Zhang, T. Xu, Y. Zhang and D. Wang, *Int. J. Nanomed.*, 2016, **11**, 5671.
24 S. Melemenidis, A. Jefferson, N. Ruparelia, A. M. Akhtar, J. Xie, D. Allen, A. Hamilton, J. R. Larkin, F. Perez-Balderas, S. C. Smart, R. J. Muschel, X. Chen, N. R. Sibson and R. P. Choudhury, *Theranostics*, 2015, **5**, 515.

25 F. Zhang, X. Huang, L. Zhu, N. Guo, G. Niu, M. Swierczewska, S. Lee, H. Xu, A. Y. Wang, K. A. Mohamedali, M. G. Rosenblum, G. Lu and X. Chen, *Biomaterials*, 2012, **33**, 5414.
26 F. C. Gaertner, H. Kessler, H.-J. Wester, M. Schwaiger and A. J. Beer, *Eur. J. Nucl. Med. Mol. Imaging*, 2012, **39**, S126.
27 M. Mammen, S.-K. Choi and G. M. Whitesides, *Angew. Chem., Int. Ed.*, 1998, **37**, 2754.
28 G. Thumshirn, U. Hersel, S. L. Goodman and H. Kessler, *Chem. – Eur. J.*, 2003, **9**, 2717.
29 Y. Wu, X. Z. Zhang, Z. M. Xiong, Z. Cheng, D. R. Fisher, S. Liu, S. S. Gambhir and X.-Y. Chen, *J. Nucl. Med.*, 2005, **46**, 1707.
30 I. Dijkgraaf, A. Y. Rijnders, A. Soede, A. C. Dechesne, G. Wilma van Esse, A. J. Brouwer, F. H. M. Corstens, O. C. Boerman, D. T. S. Rijkers and R. M. J. Liskamp, *Org. Biomol. Chem.*, 2007, **5**, 935.
31 S. Chakraborty, J. Shi, Y.-S. Kim, Y. Zhou, B. Jia, F. Wang and S. Liu, *Bioconjugate Chem.*, 2010, **21**, 969.
32 D. J. Welsh and D. K. Smith, *Org. Biomol. Chem.*, 2011, **9**, 4795.
33 D. Boturyn, J.-L. Coll, E. Garanger, M.-C. Favrot and P. Dumy, *J. Am. Chem. Soc.*, 2004, **126**, 5730.
34 C. H. F. Wenk, F. Ponce, S. Guillermet, C. Tenaud, D. Boturyn, P. Dumy, D. Watrelot-Virieux, C. Carozzo, V. Josserand and J.-L. Coll, *Cancer Lett.*, 2013, **334**, 188.
35 S. D. Robinson, L. E. Reynolds, V. Kostourou, A. R. Reynolds, R. G. da Silva, B. Tavora, M. Baker, J. F. Marshall and K. M. Hodivala-Dilke, *J. Biol. Chem.*, 2009, **284**, 33966.
36 S. Koch, L. A. van Meeteren, E. Morin, C. Testini, S. Westrom, H. Bjorkelund, S. Le Jan, J. Adler, P. Berger and L. Claesson-Welsh, *Dev. Cell*, 2014, **28**, 633.
37 R. Soldi, S. Mitola, M. Strasly, P. Defilippi, G. Tarone and F. Bussolino, *EMBO J.*, 1999, **18**, 882.
38 S. D. Robinson, L. E. Reynolds, V. Kostourou, A. R. Reynolds, R. G. da Silva, B. Tavora, M. Baker, J. F. Marshall and K. M. Hodivala-Dilke, *J. Biol. Chem.*, 2009, **284**, 33966.
39 A. R. Reynolds, I. R. Hart, A. R. Watson, J. C. Welti, R. G. Silva, S. D. Robinson, G. Da Violante, M. Gourlaouen, M. Salih, M. C. Jones, D. T. Jones, G. Saunders, V. Kostourou, F. Perron-Sierra, J. C. Norman, G. C. Tucker and K. M. Hodivala-Dilke, *Nat. Med.*, 2009, **15**, 392.
40 A. R. Reynolds, L. E. Reynolds, T. E. Nagel, J. C. Lively, S. D. Robinson, D. J. Hicklin, S. C. Bodary and K. M. Hodivala-Dilke, *Cancer Res.*, 2004, **64**, 8643.
41 S. Zanella, M. Mingozzi, A. Dal Corso, R. Fanelli, D. Arosio, M. Cosentino, L. Schembri, F. Marino, M. De Zotti, F. Formaggio, L. Pignataro, L. Belvisi, U. Piarulli and C. Gennari, *ChemistryOpen*, 2015, **4**, 633.
42 N. Papo, A. P. Silverman, J. L. Lahti and J. R. Cochran, *Proc. Natl. Acad. Sci. U. S. A.*, 2011, **108**, 14067.
43 G. Y. Perreta, A. Starzec, N. Hauet, J. Vergote, M. Le Pecheur, R. Vassy, G. Léger, K. A. Verbeke, G. Bormans, P. Nicolas, A. M. Verbruggen and J.-L. Moretti, *Nucl. Med. Biol.*, 2004, **31**, 575.
44 M. Galibert, O. Renaudet, P. Dumy and D. Boturyn, *Angew. Chem., Int. Ed.*, 2011, **50**, 1901.
45 V. Hong, S. I. Presolski, C. Ma and M. G. Finn, *Angew. Chem., Int. Ed.*, 2009, **48**, 9879.
46 Y. Ye and X. Chen, *Theranostics*, 2011, **1**, 102.
47 Y. Cheng, C. Sun, X. Ou, B. Liu, X. Lou and F. Xia, *Chem. Sci.*, 2017, **8**, 4571.
48 Y. Ma, S. Liang, J. Guo and H. Wang, *J. Radioanal. Nucl. Chem.*, 2016, **308**, 741.
49 Y. Ma, S. Liang, J. Guo, R. Guo and H. Wang, *J. Labelled Compd. Radiopharm.*, 2014, **57**, 627.